International Journal of Pharmaceutics 363 (2008) 66–72

Contents lists available at ScienceDirect

International Journal of Pharmaceutics

journal homepage: www.elsevier.com/locate/ijpharm

Simultaneous measurement of liquid-phase and solid-phase transformation kinetics in rotating disc and channel flow cell dissolution devices

Paula Lehto[a,b,*], Jaakko Aaltonen[a], Pentti Niemelä[c], Jukka Rantanen[d], Jouni Hirvonen[a], Veli Pekka Tanninen[b], Leena Peltonen[a]

[a] Division of Pharmaceutical Technology, University of Helsinki, P.O. Box 56, FI-00014 Helsinki, Finland
[b] Orion Corporation, Orion Pharma, P.O. Box 65, FI-02101 Espoo, Finland
[c] VTT, Optical Instrument Centre, P.O. Box 1100, FI-90571 Oulu, Finland
[d] Department of Pharmaceutics and Analytical Chemistry, Faculty of Pharmaceutical Sciences, University of Copenhagen, Copenhagen, Denmark

ARTICLE INFO

Article history:
Received 13 December 2007
Received in revised form 2 July 2008
Accepted 5 July 2008
Available online 15 July 2008

Keywords:
Dissolution rate
Solid state
Raman spectroscopy
Polymorphism
Hydrates/solvates
Rotating disc
Channel flow cell
Simulated gastric fluid

ABSTRACT

Solvent-mediated solid-phase transformations may occur during dissolution tests which complicates the evaluation of dissolution rates in cases of metastable drugs. The purpose of this study was to determine the effects of solvent-mediated transformations of theophylline anhydrate (TP (A)) on the intrinsic dissolution rate in simulated gastric fluid at pH 1.2. A combined method set-up for simultaneous measurement of the dissolved quantity of drug and the solid form composition was constructed from *in situ* Raman spectroscopy and UV–vis-spectrophotometry. Transformation kinetics in the traditional USP rotating disc (RD) dissolution apparatus was compared with the recently introduced channel flow cell (CFC). Solid-phase data, supported by scanning electron micrographs taken off-line, explained the changes in the intrinsic dissolution rates due to hydrate formation. Kinetic modelling showed that first order kinetics fitted the data in CFC, but the conversion in RD was strongly S-shaped. These differences were related to dissimilar hydrodynamic conditions and diffusion characteristics in the two dissolution testing devices. *In situ* solid-phase measurement during dissolution testing can largely improve the understanding of the dissolution results of metastable drugs. This information is valuable in drug candidate selection as well as in explaining and controlling the behaviour of drug substances in the final drug products.

1. Introduction

Dissolution testing has many critical roles during the various stages of drug product development (Dressman and Krämer, 2005; FDA, 1997). The need to demonstrate the dissolution consistency among pure active pharmaceutical ingredients (API) has risen due to changes in the bulk active synthesis, the final crystallization steps, particle size and surface area, polymorphism and scale-up issues regarding batch-size and manufacturing site (ICH, 2000; FDA, 2007; Brittain, 1999; Vippagunta et al., 2001). For example, crystal polymorphism is a single physical property, the fluctuation of which is estimated to be the cause for irrational dissolution and absorption behaviour of many poorly soluble drugs, such as carbamazepine and ritonavir (Meyer et al., 1992; Chemburkar et al., 2000). A real challenge in this field is that a metastable crystal form may undergo a solvent-mediated polymorphic phase transformation to a thermodynamically more stable solid form during the dissolution (Shefter and Higuchi, 1963). A transformation from an anhydrate (higher solubility) drug to a hydrate (lower solubility) form, for example, decreases the dissolution rate and depletes the drug concentration available for absorption *in vivo*.

At the moment, also the regulatory climate is strongly encouraging in understanding drug product performance from a more science-based perspective (ICH Q8, 2005). The quality-by-design approach (QBD) initiated by the FDA is an example of how the quality should be 'built step by step to the end product' (ICH Q9, 2005). The first step in order to fully understand the dissolution behaviour of a drug product is the clarification of the intrinsic dissolution behaviour of the pure API. However, the traditionally used measurement of dissolved amounts cannot alone explain the problematic dissolution behaviour of API's that can undergo solvent-mediated conversion during the dissolution. Thus, new approaches in this field are needed.

Solvent-mediated transformations can be described by three stages (Cardew and Davey, 1985). (1) A pre-transformation stage

* Corresponding author at: Division of Pharmaceutical Technology, University of Helsinki, P.O. Box 56, FI-00014 Helsinki, Finland. Tel.: +358 10 426 3203; fax: +358 10 426 2024.
E-mail address: paula.lehto@orionpharma.com (P. Lehto).

0378-5173/$ – see front matter © 2008 Elsevier B.V. All rights reserved.
doi:10.1016/j.ijpharm.2008.07.001

during which a local supersaturation is created by the dissolution of the metastable form; (2) During the transformation stage the nucleation and growth of the stable phase and dissolution of both phases occur; (3) After the transformation is over (steady-state stage), the crystals of the stable form dissolve at a constant rate. The basis of the intrinsic dissolution method is that the surface area usually regulated by forming a compact is kept constant during testing (Levich, 1962; USP 30, 2007). The uncontrollable surface area caused by crystal growth of the stable solid form will, thereby, lead to serious drawbacks in the dissolution rate evaluation. Moreover, the concentration gradient at the solid–liquid interface that is kinetically controlling the dissolution and growth rates is known to be affected by the method dependent parameters, such as temperature, composition of dissolution medium, viscosity, nature of liquid flow and agitation speed (Igimi and Carey, 1981; Grijseels et al., 1982; Nicklasson et al., 1988). However, the actual effect of these factors on the crystallization kinetics has not been clarified thoroughly.

In this study, in-depth analyses of the solvent-mediated transformation kinetics of theophylline (TP) were determined during intrinsic dissolution tests. In past studies, solvent-mediated transformation has been characterized mostly using off-line techniques (Rodriquez-Hornedo and Murphy, 2004; Tian et al., 2007), which, however, are incapable of quantifying the fast converting phases. Recently, successful applications of Raman spectroscopy have been reported in the characterization of polymorphic transformations in aqueous surroundings and in linking the solid- and liquid-phase events during dissolution testing in water (Aaltonen et al., 2006; Sandler et al., 2007). Here, the *in situ* Raman measurements were utilized for the first time to evaluate solvent-mediated transformation kinetics with the most used intrinsic dissolution device, standardized rotating disc (RD) (USP 30, 2007). Also the feasibility of Raman measurements in a biorelevant medium was demonstrated. In addition to the RD, channel flow cell (CFC) dissolution device (Compton et al., 1993; Peltonen et al., 2003) was used to evaluate the influence of the device and methodology of the results. Kinetic modelling of the hydrate formation allowed detailed determinations of transformation mechanisms and kinetics in the two devices.

2. Experimental

2.1. Drug substances

Theophylline (TP) (anhydrate form (TP (A))) was supplied by Orion Pharma (Orion Corporation, Finland). Theophylline has been reported to undergo solvent-mediated phase transformation from anhydrate to monohydrate form in aqueous surroundings (Shefter and Higuchi, 1963; de Smidt et al., 1986). The monohydrate form is the stable form in water. Theophylline monohydrate (TP (M)) was prepared by the recrystallization of TP from purified water. Theophylline anhydrate was obtained by dehydration of TP (M) at 100 °C under reduced pressure (72 mbar) for 24 h to ensure complete transformation. Samples of TP (M) and (A) forms were stored at room temperature and in 75 and 0% relative humidities, respectively. XRPD was employed to ensure the solid-phase composition immediately before the dissolution experiments.

2.2. Dissolution testing

2.2.1. Rotating disc (RD) apparatus (USP apparatus VI)

Dissolution studies were carried out using a rotating disc apparatus developed by VTT Optical Instrument Centre (dimensions according to the USP (USP 30, 2007); VTT, Finland). Drug powder samples were compressed (12-ton E-Z Press, ICL, USA) in a die (compact weight 120 mg, ø 0.8 cm, $A = 0.5\ cm^2$). In each case XRPD was used to check crystallinity after compression. The rotation rate was 50 rpm. To test if our rotating disc set-up agreed with the theoretical predictions (Levich, 1962; Grijseels et al., 1982), the surface specific dissolution rate as a function of angular velocity was measured (rotation rates: 50, 75, 100 and 150 rpm).

2.2.2. Channel flow cell (CFC) apparatus

A detailed description of the apparatus can be found in the publication of Peltonen et al. (2003). Compacts were formed by compressing 150 mg of drug powder using a single punch tablet machine (Korsch EK0, Erweka Apparatebau, Germany) with flat-faced punches (ø 0.9 cm, $A = 0.64\ cm^2$). Crystallinity was checked by XRPD in these cases as well. The flow rate of the dissolution medium was 9.5 ml/min.

Simulated Gastric Fluid pH 1.2 (USP, without enzymes) supplied by Reagena (Oy Reagena Ltd., Finland) was used as the dissolution medium (500 ml, 37 °C). The concentrations were measured using flow-through cuvettes at a wavelength of 272 nm. Sink conditions were maintained throughout all the dissolution experiments.

2.3. Solid state analysis

2.3.1. Raman spectroscopy

Schematic pictures of rotating disc and channel flow cell set-ups illustrating the positions of the Raman probe in each measuring configuration are presented in Fig. 1.

2.3.1.1. Rotating disc set-up (Raman spectrometer 1). Raman spectra were measured using a CCD-Raman spectrometer ($8\ cm^{-1}$ resolution) developed by VTT Optical Instrument Centre (Finland). An 830 nm laser was focused on the sample through a fibre-optic probe (laser spot size 600 μm (diam.), laser power 150 mW). Each spectrum obtained required a scan with an integration time of 10 s. Spectra were obtained every minute. The Raman signal was measured outside of the dissolution vessel. Therefore, to access the compact surface, the signal had to travel 3 cm through the dissolution medium and the glass wall of the vessel and 2 cm through the water bath.

2.3.1.2. Channel flow set-up (Raman spectrometer 2). A Raman spectrometer ($5\ cm^{-1}$ resolution; Control Development Inc., IN) equipped with a fibre-optic probe (laser spot size 200 μm, focal length 10 mm; InPhotonics, Norwood, MA) and a diode laser (wavelength 785 nm; Starbright 785 S, Torsana Laser Technologies, Denmark) were used in the channel flow cell set-up. The Raman signal was measured through a quartz sight window. Each spectrum was composed of three scans with a minimum integration time of 1 s per scan. Spectra were obtained every 10 s over the duration of the experiments.

2.3.1.3. Solid-phase quantification. Solid-phase quantification method was generated using TP (A)–TP (M) binary powder mixture samples. Samples with a mass of 1 g were geometrically mixed to achieve uniform physical mixtures at 10 or 20% (w/w) increments from 0 to 100% anhydrate form into hydrate form. Since the calibration models using dry powder mixtures have been found to be accurate in quantification of the polymorphic conversions *in situ* in aqueous surroundings (Ono et al., 2004; Aaltonen et al., 2006), it was considered a suitable approach for this study. The samples were prepared in triplicate and the Raman spectra were measured immediately after preparation. To avoid sub-sampling, the sample vial was rotated (50 rpm) during measurement. Characteristic peaks of both the polymorphic forms were identified. A ratio of peak areas was calculated for each calibration sample and

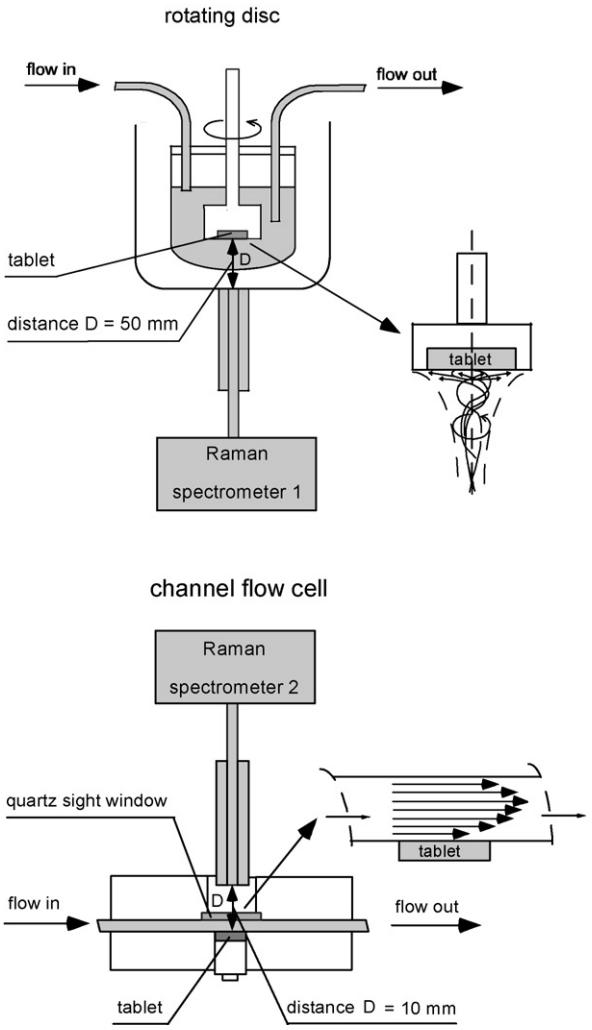

Fig. 1. Schematic illustrations of (a) RD and (b) CFC set-ups. Direction of liquid flow is illustrated in the figures.

the results were correlated with the hydrate content (w/w%) in the samples. The spectra were preprocessed by standard normal variate (SNV) correction before the peak comparisons (Barnes et al., 1989). Calibration models prepared for the purpose of quantitation produced acceptable linear functions; the correlation coefficients (R^2) and the root mean standard error of prediction (RMSEP) were 0.9881 and 8.0% (Raman 1) and 0.9995 and 0.8% (Raman 2), respectively.

2.3.2. X-ray powder diffraction (XRPD)

The prepared anhydrate and hydrate forms of the TP crystals and compacts (before and immediately after the dissolution tests), as well as the reliability of Raman determinations, were verified by X-ray powder diffraction (D8 Advance, Bruker AXS, Germany). Measurements were taken in the symmetrical reflection mode with Cu Kα radiation (1.54 Å) using Göbel mirror bent multilayer optics. The X-ray generator was set at an acceleration voltage of 40 kV and a filament emission of 40 mA. The diffraction patterns were collected over the range of 5–35° (2θ) at a step size of 0.05° (2θ) (t = 1 s/step), using an aluminum sample holder.

2.3.3. Scanning electron microscopy (SEM)

SEM micrographs were taken of the compact surfaces before and after 6, 12 and 30 min of dissolution in the rotating disc set-up and 2, 4 and 8 min of dissolution in the channel flow cell set-up (Scanning microscope JSM-840A, Jeol, Tokyo, Japan, 2.5 kV beam acceleration voltage). Samples were coated by sputter with a layer of gold under vacuum. Micrographs were recorded using a digital imaging system (ADDA and Image AnalySIS pro software, Olympus Soft Imaging Solutions GmbH, Germany).

2.4. Kinetic analyses

Solid-phase data fittings were conducted by using nonlinear mixed effects models (NONMEM) (Adams and Coomans, 2002) (SAS software, version 9.1.3, SAS Institute Inc., USA). The NONMEM approach was used, since it allows all the data to be modelled at the same time without the need to use average values. It takes into account the covariance structure of the data, making it superior to many other modelling techniques (for example, nonlinear regression). NONMEMs were built in the following way. First, the effects that should have an associated random component and those that should be purely fixed were determined. Secondly, the structured random effects variance–covariance matrix was selected. The Weibull distribution was chosen because of its flexibility and meaningful interpretation of its parameters. This model, by using non-linear mixed effects, can be expressed as:

$$frac_{ij} = (X_{0(\infty)} + X_{1(\infty)}Setup_i + u_{1i}) \times \left(1 - \exp\left(\left(\frac{-T_{ij}}{\alpha_0 + \alpha_1 Setup_i + u_{2i}}\right)^{\beta_0+\beta_1 Setup_i}\right)\right) + \varepsilon_{ij}, \quad (1)$$

where $frac_{ij}$ is the % of TP (M) and T_{ij} is the time at time point j for compact i. $Setup_i$ is the indicator variable (is given a value 0 in case of RD and a value 1 in case of CFC), $X_{0(\infty)}$ is the % of TP (M) at infinite time, α_0 is the scale factor (time when 63.2% has been transformed), and β_0 is the shape factor for the RD. For the CFC, the % TP (M) at infinite time is $X_{0(\infty)} + X_{1(\infty)}$, the scale factor is $\alpha_0 + \alpha_1$, and the shape factor is $\beta_0 + \beta_1$. Parameters $X_{1(\infty)}$, α_1 and β_1 represent the differences between the RD and CFC batches. Parameter ε_{ij} is the term for random errors. Random components u_{i1} and u_{i2} for % of TP (M) at infinite time and for time when 63.2% has been transformed, respectively, were assumed to be normally distributed:

$$\begin{pmatrix} u_{i1} \\ u_{i2} \end{pmatrix} \sim N\left(\begin{bmatrix} 0 \\ 0 \end{bmatrix}, \begin{bmatrix} \sigma_1^2 & \sigma_{12} \\ \sigma_{21} & \sigma_2^2 \end{bmatrix}\right) \qquad \varepsilon_{ij} \sim N(0, \Sigma_i).$$

Rate of conversion functions were solved by taking the first derivative of the fitted Weibull models. Because very small changes in the rate parameter could be covered by variation, the rate of 2% per minute was chosen as a limit for the progression of conversion. The induction time ($T_{\text{induction}}$) and the time to reach the steady state of conversion ($T_{\text{steady state}}$) were solved from the functions:

$$\mathrm{d}(frac_{ij}) = 2\%/\min \quad (2)$$

The time point when transformation started to slow down, T_{sl}, was calculated according to the following equation:

$$T_{sl} = (\alpha_0 + \alpha_1 Setup_i)\left(\frac{((\beta_0 + \beta_1 Setup_i) - 1)}{\beta_0 + \beta_1 Setup_i}\right)^{1/(\beta_0+\beta_1 Setup_i)} \quad (3)$$

Furthermore, the time point when half of TP (A) had transformed to TP (M) (%) form, $T_{50\%}$, was calculated:

$$T_{50\%} = (\alpha_0 + \alpha_1 Setup_i)(\log 2)^{1/(\beta_0+\beta_1 Setup_i)} \quad (4)$$

The concentration data were analysed by moving the fit of a simple linear regression (SAS software, version 9.1.3, SAS Institute Inc., USA). The series of regression coefficients were considered estimates of the rate of dissolution.

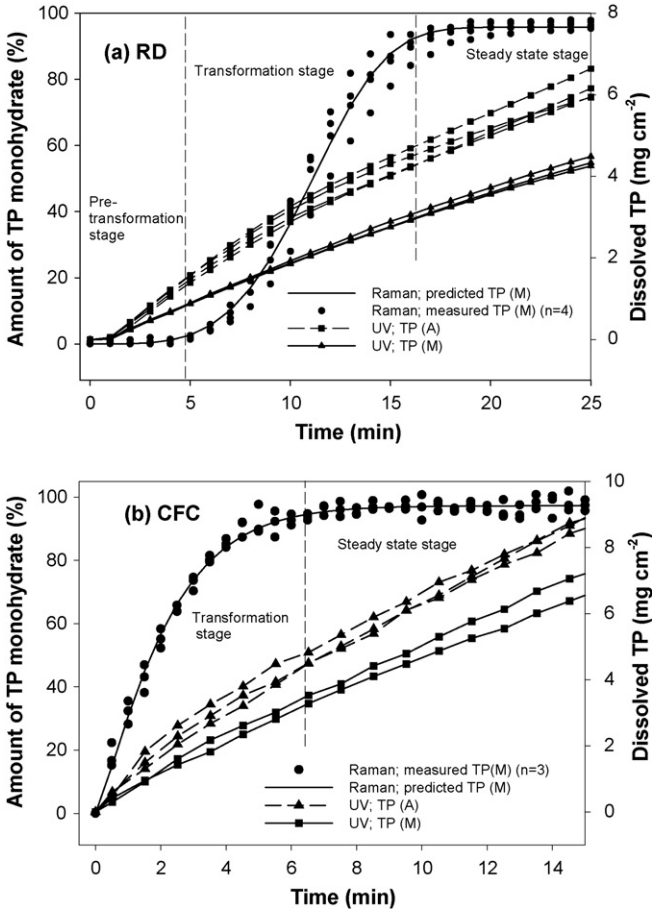

Fig. 2. Results of the intrinsic dissolution tests of TP (A) compacts in (a) RD and (b) CFC. Solid-state composition (%) measured by Raman spectroscopy is shown in the primary *y*-axis and the amount of dissolved material (mg cm^{-2}) is shown in the secondary *y*-axis. Dissolved material (mg cm^{-2}) of TP (M) compacts is also demonstrated as a reference.

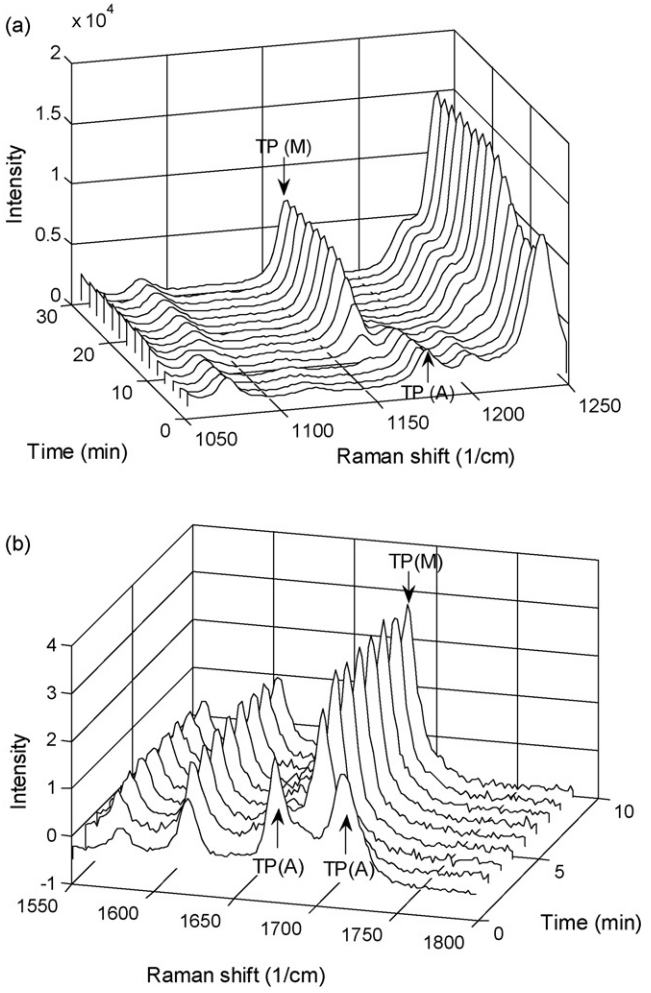

Fig. 3. Waterfall plot of Raman spectra collected during intrinsic dissolution testing in (a) RD and (b) CFC showing the transformation of TP (A) to TP (M) form. Characteristic peaks used in quantitation are marked in figures: (a) 1150–1200 cm^{-1} and (b) 1670–1720 cm^{-1}.

3. Results and discussion

The effects of hydrate formation during the intrinsic dissolution testing of TP (A) were studied in detail within and between the two different dissolution devices, rotating disc (RD) and channel flow cell (CFC). The responses were (1) solid state changes measured by *in situ* Raman spectroscopy, (2) dissolved amount of drug over time, measured with UV-spectrophotometry, and (3) crystal growth, measured with SEM.

Fig. 2a and b demonstrate the effects of the increasing hydrate ratio on the intrinsic dissolution rate of the initially anhydrous TP (A) compacts. In both the devices, the TP (A) was transformed

Table 1
Descriptive solid transformation (from TP (A) to TP (M)) and liquid state parameters for RD and CFC

Solid state parameters			Liquid state parameters		
	RD (mean (95% CI))	CFC (mean (95% CI))		RD (mean (S.D.))	CFC (mean (S.D.))
CBZ (A)			CBZ (A)		
$T_{induction}$ (min)[a]	4.9	0	IDR_{ind} (mg cm^{-2} min^{-1})[e]	0.38 (0.02)	1.14 (0.21)
$T_{steady\ state}$ (min)[b]	16.6	6.3	IDR_{steady} (mg cm^{-2} min^{-1})[f]	0.21 (0.01)	0.55 (0.03)
T_{sl} (min)[c]	11.2 (10.4, 12.0)	0.5 (0, 2.3)	$T_{linearized}$ (min)[g]	13	6
$T_{50\%}$ (min)[d]	11.0 (10.2, 11.7)	1.7 (1.2, 2.2)			
Unconverted CBZ(A) (%)	4.2 (3.4, 5.0)	2.7 (2.1, 3.4)	CBZ (D)		
Max. rate (%/min)	12.4 (9.8, 14.9)	32.7 (19.7, 45.7)	IDR (mg cm^{-2} min^{-1})	0.18 (0.01)	0.44 (0.03)

[a] $T_{induction}$, Duration of induction time.
[b] $T_{steady\ state}$, Start of steady state stage of conversion.
[c] T_{sl}, Start of conversion rate slowdown.
[d] $T_{50\%}$, Time point when 50% has converted to TP (M).
[e] IDR_{ind}, Intrinsic dissolution rate during induction period.
[f] IDR_{steady}, Intrinsic dissolution rate during steady state stage.
[g] $T_{linearized}$, Start of linearized phase of intrinsic dissolution rate.

completely to monohydrate form. There was minimal deviation between the replicates, which indicated regular occurrence of the conversion as well as repeatability of the dissolution and solid-phase monitoring methods. The *in situ* evaluation of the conversion, however, was shown to be much more challenging in the case of RD. The changes at the wavenumbers where clear spectral differences during the dissolution experiments existed are presented in Fig. 3a and b. In the case of CFC, TP (A) had distinct peaks at 1671 and 1714 cm^{-1} and TP (M) had a characteristic peak at 1694 cm^{-1}. However, in the RD, the use of those peaks was not possible due to a decreased signal-to-noise ratio at the high wavenumber end of the spectrum. The intensity of the Raman signal was decreased probably as a result of light interactions while passing through the layers of water and glass between the sample and the probe. This effect was clearly lower in the range of 1150–1200 cm^{-1}, and the use of these peaks in the quantification was considered to give reliable results. The verification of the phase change with XRPD supported the spectroscopic data by showing that X-ray diffractograms of the compacts were similar to TP (M).

A more detailed description on how the hydrate crystallization affected the dissolution rate is shown in Fig. 4a and b. The solid-phase data was utilized to distinguish the three stages of solvent-mediated conversions previously described (Cardew and Davey, 1985) and illustrated in the Fig. 4a and b. The calculated descriptive solid- and liquid-phase parameters in each of these phases are compiled in Table 1. Raman data was shown to explain the changes in dissolution rates extremely well. It was clearly demonstrated that the three-fold higher dissolution rate in the CFC device (0.38 ± 0.02 and 1.14 ± 0.21 mg cm^{-2} min^{-1} in RD and CFC, respectively) during the pre-transformation phase was reflected in the onset of the crystallization. This implication is understandable, since the higher dissolution rate promotes the attainment of supersaturation prior to nucleation. Moreover, the slower decrease in the dissolution rate in the RD device was linked to the lower rate of conversion (max. rate ~12%/min and ~33%/min in the RD and CFC, respectively). The results in the CFC are well in line with our previous study in which the solvent-mediated transformations of TP were analysed in water (Aaltonen et al., 2006). It should be noted that Raman was not able to measure only the outermost molecular layers where dissolution, nucleation and growth occurred. In fact, the depth of Raman measurement has recently been reported to vary from few hundred micrometers to one millimetre (Matousek, 2007). This explains the slight discrepancies between the solid and liquid state data.

Modelling of the kinetics confirmed that the transformation in the CFC clearly followed the first order kinetics, but the transformation kinetics in the RD was sigmoidal (goodness of fit values are illustrated in Fig. 2a and b). The shape parameters β, from the Weibull model, were 4.1 and 1.2 for RD and CFC, respectively ($\beta = 1$ first-order or exponential, $\beta > 1$ S-shaped, $\beta < 1$ initially faster than first-order or exponential). The sigmoidal transformation profile in the RD was mainly due to an inadequate mixing character, primarily low rotation rate (50 rpm), which was probably insufficient to promote the intermolecular collisions near the solid–liquid interface that could set up rapid nucleation and growth. In fact, the solid-phase transformation in RD also followed the first order kinetics after the induction period was over and the conversion was clearly underway. The dissolution rates with rotation speeds 50, 75, 100 and 150 rpm obtained during the induction period were shown to depend linearly on the square root of the rotation speed ($R^2 = 0.9984$, zero intercept) indicating, according to Levich's theory (Levich, 1962), that the dissolution was diffusion-controlled. Accordingly, the transport process could be accelerated and, thereby, the induction time shortened by increasing the agitation speed.

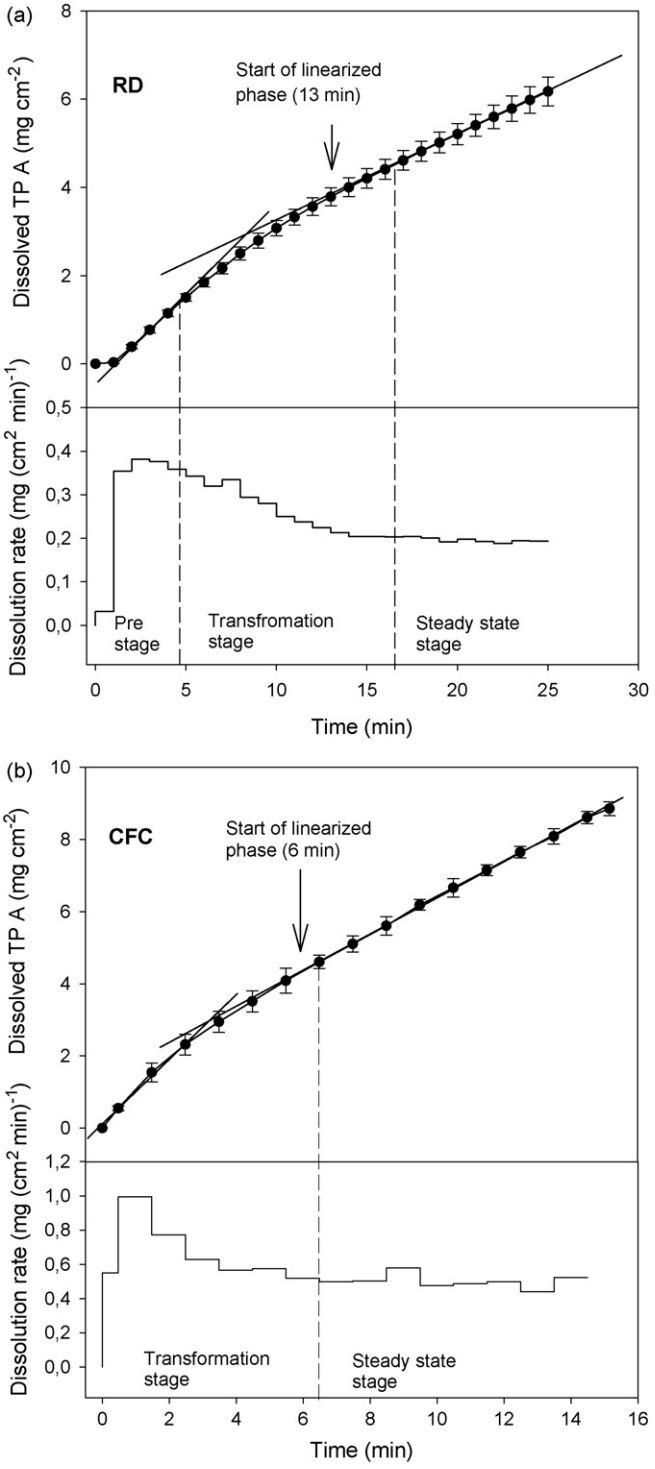

Fig. 4. Dissolution results of TP (A) in (a) RD and (b) CFC. Dissolved amounts (mg cm^{-2}) are shown in the upper parts of the figures and dissolution rates (mg cm^2 $min)^{-1}$) are illustrated in the lower parts of the figures. Dashed lines indicate the transformation stages calculated according to the solid-phase transformation data.

The conversion rates derived from the kinetic models were drawn as a function of time (Fig. 5). A period during which the dissolution and growth rates were practically balanced and the supersaturation was maintained on a plateau level (plateau supersaturation (Cardew and Davey, 1985), meaning the change in transformation rate <0.5%/min) seemed to have evolved only in the

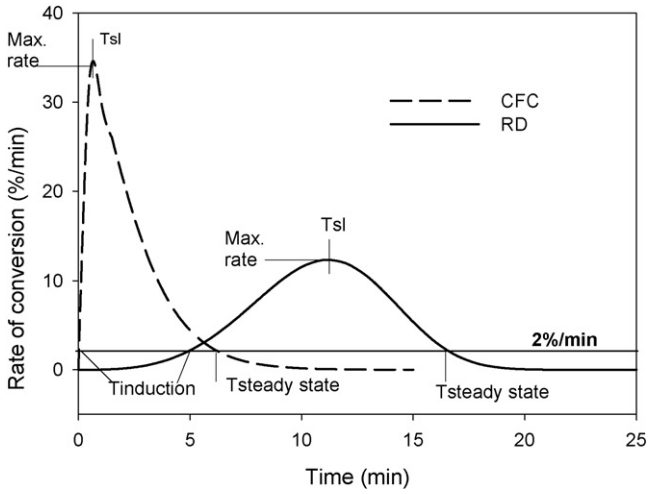

Fig. 5. Conversion-rate profiles in RD and CFC. Descriptive parameters: $T_{induction}$ (induction time), $T_{steady\ state}$ (steady state stage of conversion), T_{sl} (start of conversion rate slowdown) and maximum rate of conversion are illustrated in the figure. 2%/min was chosen as a limit for the progression of the conversion.

RD device. The layer of supersaturation (δ_S) adjacent to the solid surface is, according to a basic assumption, part of the diffusion layer (δ_D). Therefore, all the factors affecting the properties of this layer, such as agitation speed/flow rate, direction of liquid flow, also control the supersaturation. In fact, the hydrodynamic characters among the RD and the CFC are quite diverse. As illustrated in Fig. 1a, the rotating disc device provides radial and tangential motions of the liquid flow, and a boundary diffusion layer is formed at the centre (Grijseels et al., 1982). In contrast, the laminar liquid convection in the CFC device is directed parallel to the solid surface, and this has previously been demonstrated to prevent the formation of a uniform diffusion layer at the solid–liquid interface (Fig. 1b) (Compton et al., 1993). Rapid achievement of supersaturation and elevated rate of crystallization were likely assisted by this convection, which removed material continuously forward and replaced the channel with fresh solvent ensuring that the dissolution and nucleation continued without local solubility limitations.

The SEM-figures obtained off-line supported the *in situ* Raman results by confirming the clearly different timescales in the needle-like monohydrate crystal growth (Fig. 6a and b). Micrographs taken before the dissolution tests indicate more distinct pores, cracks and grain boundaries on the surface of the compact made for CFC. In general, those areas have likely acted as high energy spots in which the wettability and dissolution, as well as the nucleation and growth, occurred more rapidly (Grijseels et al., 1983; Murphy et al., 2002). The increase in the effective surface area is clearly seen in the dissolution results; despite the fact that the Raman results indicated ~100% conversion, the dissolution rate of initially anhydrous compacts was still slightly higher than the dissolution rate of TP (M) compact (Fig. 2a and b). This drawback underlines the importance of solid-phase and microscopic examination in the dissolution evaluation of metastable solids.

In addition to changes in the dissolution rate, the thick needle-growth eventually also changed the focus of the Raman spot away from the surface. On the other hand, the differences between the Raman devices (e.g. in the laser spot size and in the laser power) and measuring configurations (e.g. measuring distance, layer of medium between the sample and the probe, etc.) obviously also affected either the width or the depth of the measurement. However, a strong connection between the dissolution and solid transformation results refers to the fact that the Raman measurement was confined mostly to the few outermost surface layers where the dissolution occurred.

Dissolution evaluation has traditionally been based on the determination of dissolved amounts of drug *on/off-line* using HLPC and spectrophotometric methods, or more recently *in situ* using fibre optics (Dressman and Krämer, 2005). However, in the search for cause, the measurement of liquid phase can only show that there is a change between samples, but not what and/or why it has changed. This study showed the potential of the *in situ* Raman spectroscopic solid-phase analytics as a clarifying tool in understanding the intrinsic dissolution behaviour of metastable solid drugs. Raman measurements were also successfully utilized to explain the differences in the conversion kinetics due to the device dependent hydrodynamics. This knowledge is of great value when making development decisions between multiple solid forms (for example, between polymorphs, hydrates/solvates or even salt forms). It

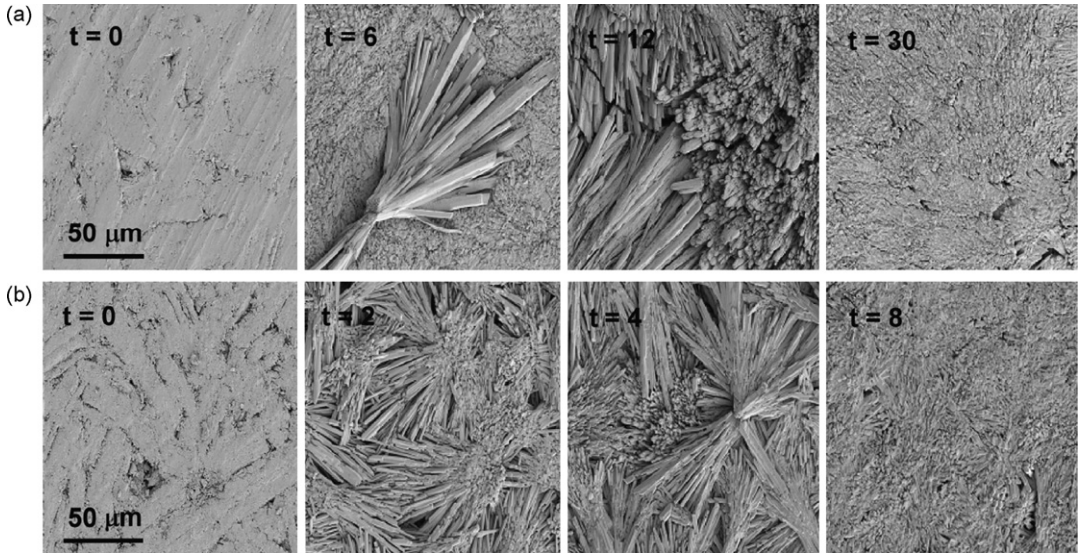

Fig. 6. Scanning electron micrographs taken off-line of the compact surfaces during dissolution testing. Growth of TP (M) needles after (a) 0, 6, 12 and 30 min of dissolution in RD and (b) 0, 2, 4 and 8 min of dissolution in CFC.

also makes the estimation of the biopharmaceutical consequences possible due to solvent-mediated conversions. Another advantage of the present method combination is that if the higher dissolution rate of a metastable solid form is desired from the absorption point of view, the composition of formulation can be planned by testing conversion-retarding excipients (Aaltonen et al., 2006).

4. Conclusions

The *in situ* Raman spectroscopic measurements during intrinsic dissolution testing enabled to explain the exceptional dissolution behaviour of theophylline. The simultaneous measurement of the solid and liquid phases showed the connection between the hydrate formation and the dissolution rate. Although Raman measurements were successfully performed in both the set-ups, very different kinetics of transformations were observed in the standardized rotating disc (USP) and channel flow cell dissolution devices. These differences were related to dissimilar dissolution and crystallization behaviour in the two set-ups, which were dictated by the hydrodynamic conditions and diffusion characteristics. The present study shows that *in situ* Raman measurements can be used to clarify the problematic intrinsic dissolution characteristics of metastable drugs. This kind of information is very valuable for the pharmaceutical industry, especially at the preformulation stage when development decisions between multiple metastable solids have to be made. Once the transformation behaviour of a pure API is clarified, its behaviour in the drug product can be evaluated and controlled.

Acknowledgements

Biostatistician Anni Liimatainen (Orion Pharma) is acknowledged for her support with the statistical issues. Dr. Osmo Antikainen (University of Helsinki) and Professor Kyösti Kontturi (Helsinki University of Technology) are acknowledged for their help with the data acquisition and with the channel flow cell dissolution equipment, respectively.

References

Adams, E., Coomans, D., Smeyers-Verbeke, J., Massart, D.L., 2002. Application of linear mixed effects models to the evaluation of dissolution profiles. Int. J. Pharm. 240, 37–53.

Aaltonen, J., Heinänen, P., Peltonen, L., Kortejärvi, H., Tanninen, V.P., Christiansen, L., Hirvonen, J., Yliruusi, J., Rantanen, J., 2006. *In-situ* measurement of solvent-mediated phase transformations during dissolution testing. J. Pharm. Sci. 95, 2730–2736.

Barnes, R.J., Dhanoa, M.S., Lister, S.J., 1989. Standard Normal Variate Transformation and de-trending of near-infrared diffuse reflectanse spectra. Applied Spectroscopy 43, 772–777.

Brittain, H.G., 1999. Polymorphism in pharmaceutical solids. Marcel Dekker, New York.

Cardew, P.T., Davey, R.J., 1985. The kinetics of solvent-mediated phase transformations. Proc. R. Soc. Lond. A 398, 415–428.

Chemburkar, S.R., Bauer, J., Deming, K., Spiwek, H., Patel, K., Morris, J., Henry, R., Spanton, S., Dziki, W., Porter, W., Quick, J., Bauer, P., Donabauer, J., Narayanan, B.A., Soldani, M., Riley, D., McFarland, K., 2000. Dealing with the impact of ritonavir polymorphs on the late stages of bulk drug process development. J. Org. Process Res. Dev. 4, 413–417.

Compton, R.C., Harding, M.S., Pluck, M.R., 1993. Mechanism of solid/liquid interfacial reactions. J. Phys. Chem. 97, 10416–10420.

Dressman, J., Krämer, J., 2005. Pharmaceutical Dissolution Testing. Taylor and Francis Group, Boca Raton, Florida.

Food and Drug Administration FDA, 1997. Guidance for Industry; Dissolution Testing of Immediate Release Solid Oral Dosage Forms.

Food and Drug Administration FDA, 2007. Guidance for Industry; ANDAs: Pharmaceutical Solid Polymorphism.

Grijseels, H., Crommelin, D.J.A., De Blaey, C.J., 1982. Hydrodynamic approach to dissolution rate. Pharm. Weekbl. Sci. Ed. 3, 129–144.

Grijseels, H., van Bloois, L., Crommelin, D.J.A., de Blaey, C.J., 1983. Dissolution at porous interfaces II. A study of pore effects through rotating disc experiments. Int. J. Pharm. 14, 299–311.

Igimi, H., Carey, M.C., 1981. Cholesterol gallstone dissolution in bile: dissolution kinetics of crystalline (anhydrate and monohydrate) cholesterol with chenodeoxycholate, ursodeoxycholate, and their glycine and taurine conjugates. J. Lipid Res. 22, 254–270.

International Conference on Harmonisation, 2000. ICH Harmonised Tripartite Guideline; Test Procedures and Acceptance Criteria for New Drug Substances and Drug Products Q6A.

International Conference on Harmonisation, 2005. ICH Harmonised Tripartite Guideline; Pharmaceutical Development Q8.

International Conference on Harmonisation, 2005. ICH Harmonised Tripartite Guideline; Quality Risk Management Q9.

Levich, V.G., 1962. Physicochemical hydrodynamics. Prentice Hall, NJ, pp. 1–184.

Matousek, P., 2007. Deep non-invasive Raman spectroscopy of living tissue and powders. Chem. Soc. Rev. 36, 1292–1304.

Meyer, M.C., Straughn, A.B., Jarvi, E.J., Wood, G.C., Pelsor, F.R., Shah, V.P., 1992. The bioinequivalence of carbamazepine tablets with a history of clinical failures. Pharm. Res. 9, 1612–1616.

Murphy, D., Rodriquez-Cintron, F., Langevin, B., Kelly, R.C., Rodriquez-Hornedo, N., 2002. Solution-mediated phase transformation of anhydrous to dihydrate carbamazepine and the effect of lattice disorder. Int. J. Pharm. 246, 121–134.

Nicklasson, M., Fyhr, P., Magnusson, A.-B., Gunnvald, K., 1988. A preformulation study on the in vitro dissolution characteristics of the organophosphorous poisoning antidote HI-6. Int. J. Pharm. 46, 247–254.

Ono, T., ter Horst, J.H., Jansens, P.J., 2004. Quantitative measurement of the polymorphic transformation of L-Glutamic Acid. Cryst. Growth Des. 4, 1161–1167.

Peltonen, L., Liljeroth, P., Heikkilä, T., Kontturi, K., Hirvonen, J., 2003. Dissolution testing of acetylsalicylic acid by a channel flow method—correlation to USP basket and intrinsic dissolution methods. Eur. J. Pharm. Sci. 19, 395–401.

Rodriquez-Hornedo, N., Murphy, D., 2004. Surfactant-facilitated crystallization of dihydrate carbamazepine during dissolution of anhydrous polymorph. J. Pharm. Sci. 96, 584–594.

Sandler, N., Savolainen, M., Saupe, A., Strachan, C., Rades, T., 2007. Applications of Raman spectroscopy in aqueous environments. Pharm. Technol. Eur. 19, 24–29.

Shefter, E., Higuchi, T., 1963. Dissolution behaviour of crystalline solvated and non-solvated forms of some pharmaceuticals. J. Pharm. Sci. 52, 781–791.

de Smidt, J.H., Fokkens, J.G., Grijseels, H., Crommelin, D.J.A., 1986. Dissolution of theophylline monohydrate and anhydrous theophylline in buffer solutions. J. Pharm. Sci. 75, 497–501.

Tian, F., Sandler, N., Aaltonen, J., Lang, C., Saville, D.J., Gordon, K.C., Strachan, C.J., Rantanen, J., Rades, T., 2007. Influence of polymorphic form, morphology and excipient interactions on the dissolution of carbamazepine compacts. J. Pharm. Sci. 96, 584–594.

USP 30, 2007. Intrinsic Dissolution. The United States Pharmacopeial Convention, Rockville.

Vippagunta, S.R., Brittain, H.G., Grant, D.J.W., 2001. Crystalline solids. Adv. Drug Del. Rev. 48, 3–26.